Journal of Applied Mathematics and Physics, 2026, 14(1), 384-399
https://www.scirp.org/journal/jamp
ISSN Online: 2327-4379
ISSN Print: 2327-4352

Modeling and Performance Analysis of PM6:Y6 Based Inverted Bulk Heterojunction Organic Solar Cells through SCAPS-1D Simulation

Tania Shakeeb[1], Jamil Khan[1,2*], Aziz Sarmad[2], Salman Khan[2], Aftab Ahmad[3], Niamatullah[2,4*], Alamgir Khan[1], Khalilullah[5], Muhammad Talha[6], Shamrez Khan[4]

[1]Department of Physics, Abdul Wali Khan University Mardan, Mardan, Pakistan
[2]College of Nuclear Science and Technology, Harbin Engineering University, Harbin, China
[3]Materials Laboratory, Department of Physics, COMSATS University Islamabad, Park Road, Islamabad, Pakistan
[4]Department of Physics, Baluchistan University of Information Technology, Engineering and Management Sciences Quetta, Quetta, Pakistan
[5]School of Materials Science and Engineering, Beijing Institute of Technology, Beijing, China
[6]Department of Physics, Malakand University, Chakdara, Pakistan
Email: *jamilkhan738@hrbeu.edu.cn, *niamatullah@hrbeu.edu.cn

How to cite this paper: Shakeeb, T., Khan, J., Sarmad, A., Khan, S., Ahmad, A., Niamatullah, Khan, A., Khalilullah, Talha, M. and Khan, S. (2026) Modeling and Performance Analysis of PM6:Y6 Based Inverted Bulk Heterojunction Organic Solar Cells through SCAPS-1D Simulation. *Journal of Applied Mathematics and Physics*, **14**, 384-399.
https://doi.org/10.4236/jamp.2026.141021

Received: December 14, 2025
Accepted: January 25, 2026
Published: January 28, 2026

Abstract

This study investigates the influence of active layer thickness and temperature on the performance of PM6:Y6 based organic solar cells (OSC_S). The simulation of these parameters provides valuable insights into optimizing the efficiency and understanding the behaviors of OSC_s under different operating conditions. In the investigation of active layer, thickness simulation was conducted using SCAPS-1D for OSCs based on PM6:Y6 and the J-V characterizations of the OSC_s at varies active layer thickness were analyzed. The results reveal that as the active layer thickness increases from 250 nm to 450 nm there were a notable rise in the short current circuit density (J_{sc}) from 27.12 to 31.04 mA/cm^2. This enhancement in J_{sc} was attributed to an increase in light absorption leading to generation of more excitons within the active layer. Consequently, more charge carriers were produced resulting in increased J_{sc}. It was observed that while a slight increase in V_{oc} was regarded as the active layer thickness increases from 0.954 to 0.966 V, a significant decrease in fill factor (FF) from 72.92 to 65.8% was observed beyond a critical active layer thickness of 400 nm dropping from 67.62 to 65.8%. This reduction in FF beyond the threshold of 400 nm suggested and increase in recombination rate of charge carrier. The decrease in FF indicated that a thicker active layer might result in a higher likelihood of charge carrier recombination, which led to the observed reduction in FF and, consequently, the overall performance of the OSC. Furthermore, it was observed that the J_{sc} of the OSCs increased with working tem-

perature, reaching a saturation point. However, at high temperatures, J_{sc} started to decrease. This behavior can be explained by considering the relationship between the current delivered by the cell, the number of free charge carriers generated, and their mobility. As the working temperature increased, the V_{oc} decreased from 0.96 to 0.95V. In contrast, the FF and PCE decreased from 67.6 to 65.43% and 20.25 to 19.47% respectively. Further from the Nyquist plot, it was found that the electrode resistance increases with temperature while semiconductor materials resistance decreases with working temperature, which shows the semiconducting behavior.

Keywords

Active Layer Thickness, Organic Solar Cells (OSCs), PM6:Y6, Charge Carrier Recombination, Temperature Dependence

1. Introduction

Organic solar cells (OSCs) have become among the increasingly candidate for next generation photovoltaic technologies due to their distinctive advantages such as mechanical flexibility, lightweight nature, low fabrication cost and large surface area [1] [2]. Unlike conventional inorganic counterpart OSCs depend on organic semiconductor typically conjugated polymers and small molecules that enable solution process ability and tunable optoelectronic properties through molecular engineering [3] [4]. Despite these advantages OSCs still face challenges in achieving stability and efficiency levels comparable to silicon-based technology requiring continuous effort to optimize device structures and material combinations [5] [6]. Among varies donor acceptor system the polymer on fullerene acceptor (NFA) blend of poly donor known as PM6, paired with Y6, a high performance non fullerene acceptor has demonstrated remarkable power conversion efficiencies (PCEs) exceeding 18 % in experimental reports. The PM6:Y6 system exhibits strong near infrared absorption optimal energy level alignment and enhanced charge carrier mobility making it a benchmark material pair for high efficiency OSCs [7]. However, a comprehensive grasp of ways in which different physical parameter like operating temperature interface quality and active layer thickness affect device attributes is necessary for additional performance optimization [8]. Device simulations are now essential resources for researching and improving OSCs performance prior to experimental manufacturing. An efficient way to examine how material and device characteristics affect electrical and optical behavior is using simulation platforms like solar cells capacitance simulator (SCAPS-1D). Because of its strong foundation for resolving Poisson's and continuity equations SCAPS-1D which was first created for inorganic thin film solar cells has recently been modified for simulating organic and perovskite-based devices and SCAPS-1D performs numerical simulations by self-consistently solving the fundamental semiconductor device equations [5] [9]-[11]. Under varies structural

and environmental circumstances this method enables mythological investigation of charge formation recombination kinetics and transport mechanism [12]. Compared to traditional arrangement inverted bulk Heterojunction (BHJ) topologies have drawn more interest because of their greater stability and suitability for flexible substrates [13]-[15]. The electro transport layer (ETL) and hole transport layer (HTL) are switched in inverted configuration which usually uses materials like MoO_3 or PEDOT: PSS for the HTL and ZnO for ELT [16]-[19]. This arrangement not only improves device lifetime by reducing sensitivity to oxygen and moisture but also enhances charge extraction efficiency and reduces interfacial recombination [15] [18]. Although extensive experimental research systematic studies focusing on the simulation-based optimization of PYM6:Y6 inverted BHJ OSCs remain limited [20]. Specially there is a need to investigate how active layer thickness and working temperature influence photovoltaic parameters [21]. Understanding these dependencies is crucial for predicting device performance under practical operating conditions and guiding the fabrication of high efficiency OSCs [22]. In this study, SCAPS-1D is employed to simulate and optimize the performance of PM6:Y6 based inverted heterojunction (OSCs). The effect of active layer and working temperature are systematically examined to explain their impact on charge carrier generation, transport, recombination and energy conversion efficiency [23]. Furthermore, impedance spectroscopy simulations are conducted to interpret charge transport resistance and confirm the semiconductor behavior of the device. The insights gained from this work contribute to design of more efficient and stable PM6:Y6 OSCs and provide a theoretical foundation for future experimental developments.

2. Main Parameters in Solar Cells

The open-circuit voltage (V_{oc}) is the maximum output voltage of a solar cell when the current flowing out of it is zero. The difference between photogenerated and diode recombination currents is what determines the open-circuit voltage, and can be written as [24]:

$$V_{oc} = \frac{nkT}{q}\left(\frac{I_L}{I_0}+1\right) \tag{1}$$

where n is the diode ideality factor, k is the Boltzmann constant, T is the absolute temperature, q is the elementary charge, I_L is the light-generated current, and I_0 is the reverse saturation current.

$$I_{sc} = I - I_0\left(\mathrm{e}^{\frac{qv}{kT}}-1\right) \tag{2}$$

Under short-circuit conditions ($V=0$), Eq. (2) reduces to $I_{sc} \approx I_L$, indicating that the short-circuit current is primarily governed by the photogenerated current.

The solar power at the maximum power point is the product of current and voltage (V) at the maximum power point that determines the maximum power output (P_m) of a solar cell. The association between open-circuit voltage (V_{oc}),

short-circuit current (I_{sc}), and full power output is measured in us of the fill factor (FF). The fill factor is proportional to better output power, and highly dependent on internal series resistance and recombination losses. The fill factor is computed with the help of the equation. (3) [24] [25]:

$$\mathrm{FF} = \frac{P_m}{V_{oc} \times I_{sc}} \tag{3}$$

The power conversion efficiency (η) is a critical performance parameter that represents the ratio of the maximum electrical output power to the incident optical power. It is calculated using Eq. (4) [26] [27]:

$$\eta = \frac{V_{oc} \times I_{sc} \times \mathrm{FF}}{P_{in}} \tag{4}$$

where η represent the power conversion efficiency and P_{in} is the incident light intensity, I_{sc}, FF, V_{oc} and P_{in} determine the importance of power conversion effectiveness.

Device Architecture

The functionality of organic solar cells is dependent upon electron transport layer (ETL), which plays a pivotal role in the system. Typically, the construction of electron transport layer (ETL), involves the application of a slender coating of a material that exhibits high electro transport properties such as metal oxides like TiO_2, ZnO, and SnO_2. The thickness of electron transport layer (ETL) is influenced by the type of material employed, the device design, and the deposition method. Insufficient electron transport and insufficient charge collection can be observed in the cases where electron transport layer (ETL) is excessively very thin [28] [29]. Conversely, in the event that the thickness of electron transport layer (ETL), exceeds a certain threshold it has the potential to evaluate the resistance of electron transport thereby diminishing the overall efficiency of the device. Furthermore, the thickness of electron transport layer (ETL), may exert an influence on the charge transfer and replication mechanism transpiring at the junction of the active layer and the electrode. The performance of OSCs, is significantly impacted by the presence of hole transport layer (HTL), which operates in manner analogous to electron transport layer (ETL). The hole transport layer (HTL), facilitates the movement of positively charge carriers (hole) between the electrode and the active layer thereby influencing the interface charge transfer and recombination mechanism [29]-[31]. An active anode refers to a polymer or a small molecule that serve the dual purpose of acting as both a substance donor and an acceptor. For the absorber layer PM6:Y6 was used as a hole transport material (HTM) and TiO_2 Nano rods as an electron transport material (ETM) shown in **Figure 1**. The ETL, of TiO_2 nanorods and the hole transport layer (HTL), of PEDOT: PSS, are separated by active layer. Inorganic and perovskite optoelectronics systems PEDOT: PSS is favored as hole transport layer (HTL), because in contract to other choices it may offers a plat surface on the ITO electrode [32] [33]. TiO_2 is used as electron transport

layer (ETL), because of its affordability, chemical stability and easy use in thin films productions. The proposed configuration works TiO_2 as the transport medium which has accelerated the development of durable tin iodide-based perovskite solar cells. This material is frequently utilized in commercial solar cells [34] [35]. This design offers advantages in terms of its stability, compatibility and the diffusion length of charge carriers. The present study employs SCAPS:1D, simulation to investigate the influence of diverse electrical parameters on the efficiency of TiO_2/PM6:Y6/PEDOT: PSS (Table 1).

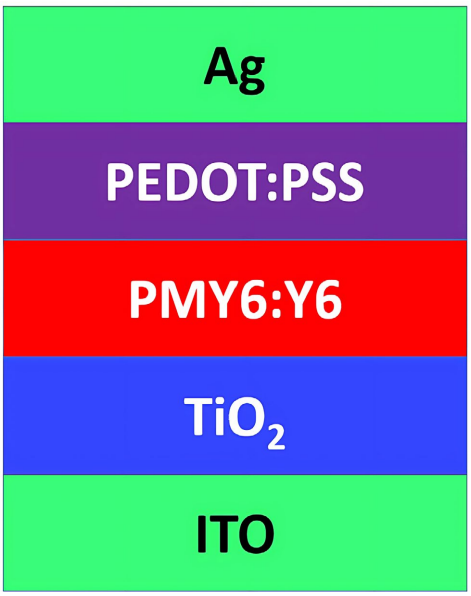

Figure 1. Device structure.

Table 1. Summarize parameters for PEDOT: PSS/ PM6:Y6/TiO_2/ITO.

Parameters	PEDOT: PSS	PM6:Y6	TiO_2	ITO
Thickness (nm)	40.0	400	50	200
Energy band gap (eV)	2.20	1.30	3.200	3.500
Electron affinity (eV)	2.90	3.45	3.900	4.0
Dielectric permittivity	3.0	3.50	9.000	9.0
CB effective density of states (cm^{-3})	2.2×10^{18}	2.2×10^{18}	2.2×10^{18}	2.2×10^{18}
VB effective density of states (cm^{-3})	1.8×10^{19}	1.8×10^{19}	1.8×10^{19}	1.8×10^{19}
Electron mobility (cm^2/Vs)	1.1×10^{1}	5.5×10^{-4}	1.1×10^{2}	20
Hole mobility (cm^2/Vs)	1.1×10^{1}	5.5×10^{-4}	2.5×10^{1}	10
Shadow acceptor density (cm^{-3})	3.17×10^{16}	1.0×10^{17}	0	0.0
Shadow donor density (cm^{-3})	0	1.0×10^{17}	9.0×10^{16}	1.0×10^{18}
Shadow donor density (cm^{-3})	0	1.0 × 1017	9.0 × 1016	1.0 × 1018

3. Results and Discussion

3.1. The Effect of Active Layer Thickness

To investigate the influence of active layer thickness of organic solar cell (OSCs) performance simulation were conducted using SCAPS-1D for OSCs based on PM6:Y6. The J-V, characteristics of the PM6:Y6 based OSCs at different active layer thickness are presented in **Figure 2**. Furthermore, **Figures 3(a)-(d)** illustrate the impact of active layer thickness on various parameters of OSCs. When the active layer thickness is increase from 250 to 450 nm, the J_{sc} show a notable rise from 27.12 to 31.05 $mAcm^{-2}$. This enhancement is attribute to a rise in light absorption, leading to generation of more excitons within the active layer [36] [37]. Consequently, a more numbers of charge carriers are produced resulting an observed increase in J_{sc} display in **Figure 3(a)**. Regarding the V_{oc} a slight increase is observed from 0.95 to 0.96 V, as the active layer thickness increases is show in **Figure 3(b)**. This change in V_{oc} is influenced by material's band gap and energy band gap alignment. The slight improvement in V_{oc} can be attributed to the specific characteristics of the PM6:Y6 based OSCs regarding their band structure alignment. However, a slight decrease in Fill factor is display in **Figure 3(c)**, when the active layer thickness exceeds 400 nm, the FF dropping from 67.62 to 65.8 %. The reduction in FF beyond the threshold of 400 nm, suggests a rise in recombination rate of charge carriers. Physically, the decrease in FF with increased active layer thickness is largely related to the increased bulk recombination processes. In the SCAPS-1D simulation system, recombination is most often modelled by Shockley-Read-Hall (SRH) trap-assisted processes, which grow more and more important as the thickness of the active layer is scaled up. The increased active layer causes the carrier transport pathways to be longer and the slowing down of the carrier residence time and, therefore, the possibility of trap-mediated recombination is high. In addition, the internal electric field also becomes weaker in the middle between thicker active layers, which decreases the effectiveness of charge extraction and causes a spatial improvement in recombination outside the electrodes. This field-dependent recombination behavior has an undesirable impact on carrier collection and hence the fill factor improves with better light absorption. The effect of both high recombination rates of SRH and lower values of the internal electric field strength can therefore explain the degradation of FF and PCE at too thick active layers. This indicates that a thickness active layer may result in a higher probability of charge carrier recombination leading to fall in FF, and therefore the overall performance of OSCs [38] [39]. Interestingly the power conversion efficiency (PCE) of OSCs also experience a decline after reaching an active layer, thickness of 400 nm, is shown in **Figure 3(d)**. As mentioned above, this decrease in PCE, is aspect to increase in charge carrier recombination rates. This responds the positive effects of the enhanced J_{sc} and the slight improvement in V_{oc}. Therefore, beyond the critical active layer thickness of 400 nm, the overall efficiency of the PM6:Y6 based OSCs reduces (**Table 2**).

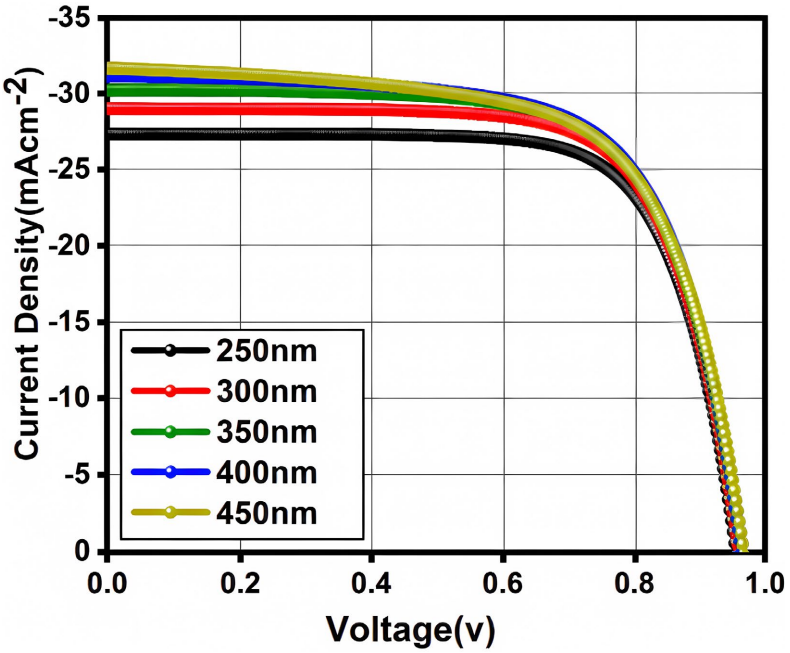

Figure 2. The influence of active layer thickness on the characteristics J-V.

Table 2. The active (absorber) layer has been taken as PM6:Y6 blend and the electron transport layer (ETL) has been taken as TiO_2 nanorods.

PM6:Y6 thickness	J_{sc} (mAcm^{-2})	V_{oc} (v)	FF (%)	PCE (%)
250 nm	27.12237	0.95422	72.92	18.87
300 nm	28.84831	0.95879	71.34	19.72
350 nm	30.13234	0.9622	69.55	20.16
400 nm	31.0497	0.9648	67.62	20.25
450 nm	31.5731	0.96683	65.80	20.08

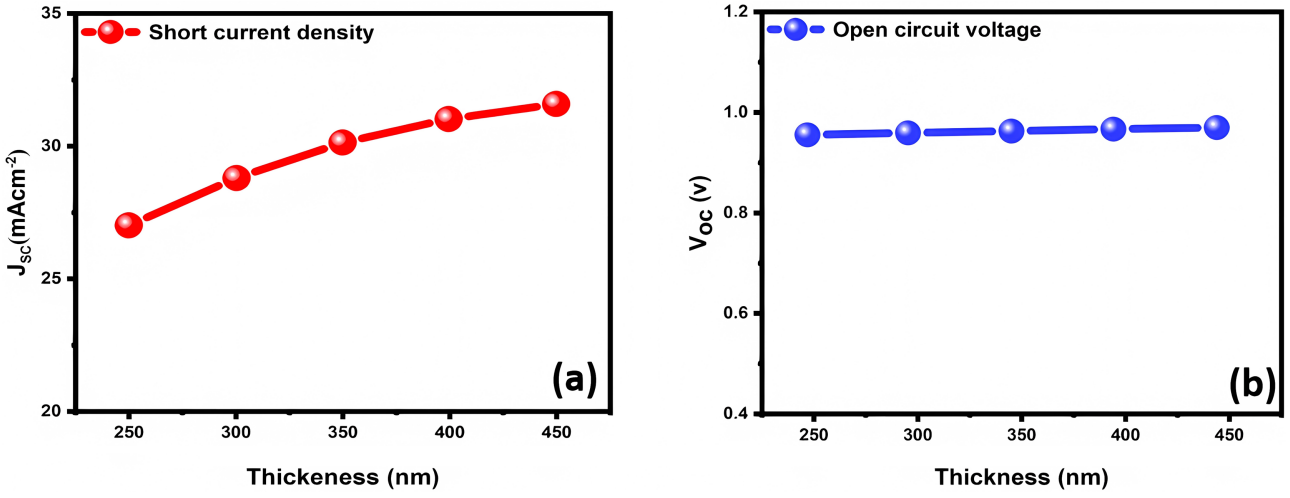

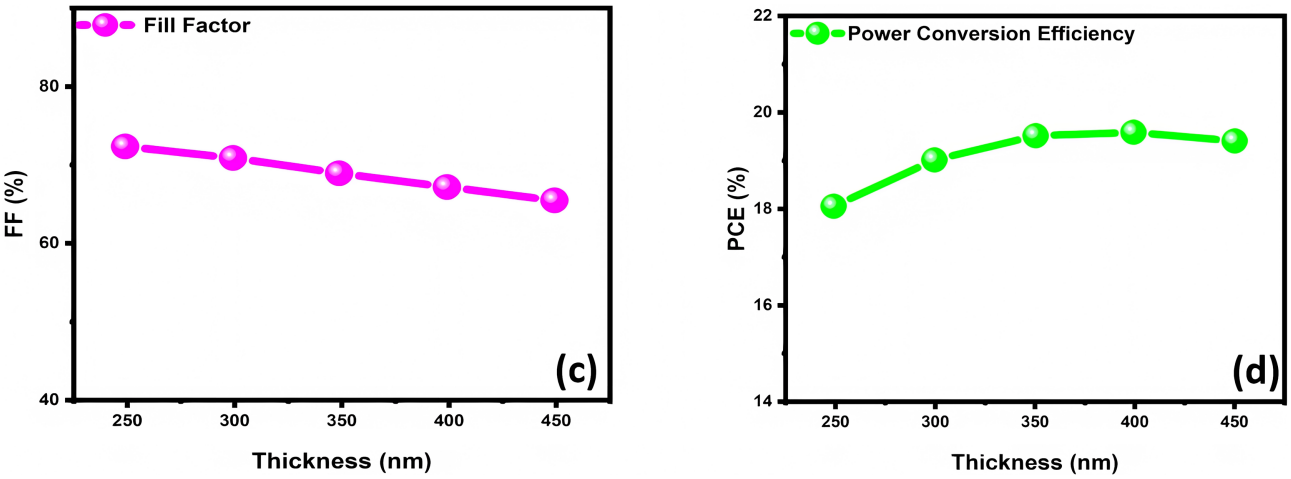

Figure 3. Influence of AL thickness on J-V characteristics, (a) J_{sc}, (b) V_{oc} (c) FF and (d) PCE.

3.2. Effect of Working Temperature on the Solar Cell Parameters

The study of the working temperature influence on OSCs performance is essential for understanding their thermal stability, given their usual exposure to temperature that span form room temperature to 330K, particularly in condition like desert summer where temperature can subsequently exceed the average. In **Figure 4**, we illustrate the effect of working temperature on J-V characteristics of OSCs. It was observed that J_{sc} increases with working temperature and reaches a saturation point at a maximum value. However, at high temperatures J_{sc} start to decrease. This behavior can be explained by considering the connection between current deliver by cell, numbers of free charge carrier generated and their mobility [40] [41]. In case of organic semiconductor, the transfer of charge carriers occurs through localize sites. The movement of charge carriers from one place to another in vicinity involved interaction with photons. The materials conductivity is thermally activated

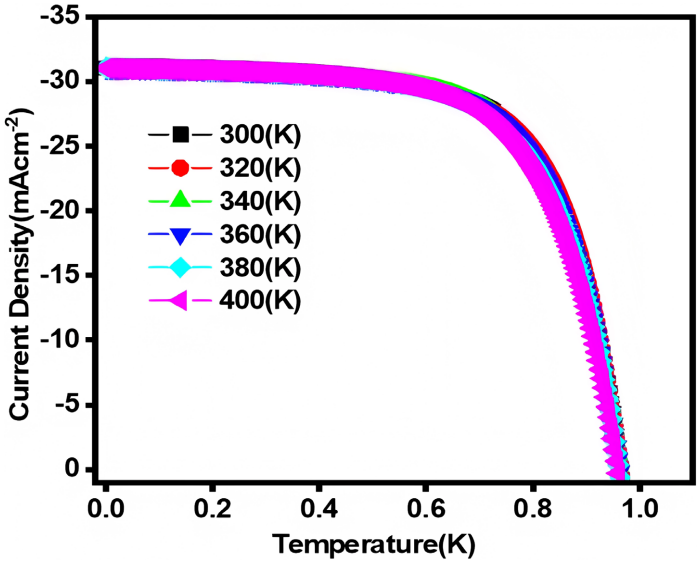

Figure 4. Influence the effect of working temperature on J-V characteristics.

increasing with temperature. This temperature dependent conductivity influences the generation and mobility of charge carrier resulting in the observed trend of J_{sc} with WT [42] [43]. Furthermore, as charge carrier concentration increases the V_{oc} will decrease due to reduction in the band gap. Optimal performance denoted by an efficiency of 20.25 % was obtained at RT. As working temperature increases from room temperature to 400K, the concentration and mobility of both electrons and holes were affected leading to fall in PCE, from 20.25 to 19.47 % is shown in Figure 5(d). The reduction in FF (67.6 to 65%) Figure 5(c), and the overall PCE, is primarily attributed to the acceleration of internal carrier recombination process within the OSCs, initiated by increases in carrier concentration (Table 3).

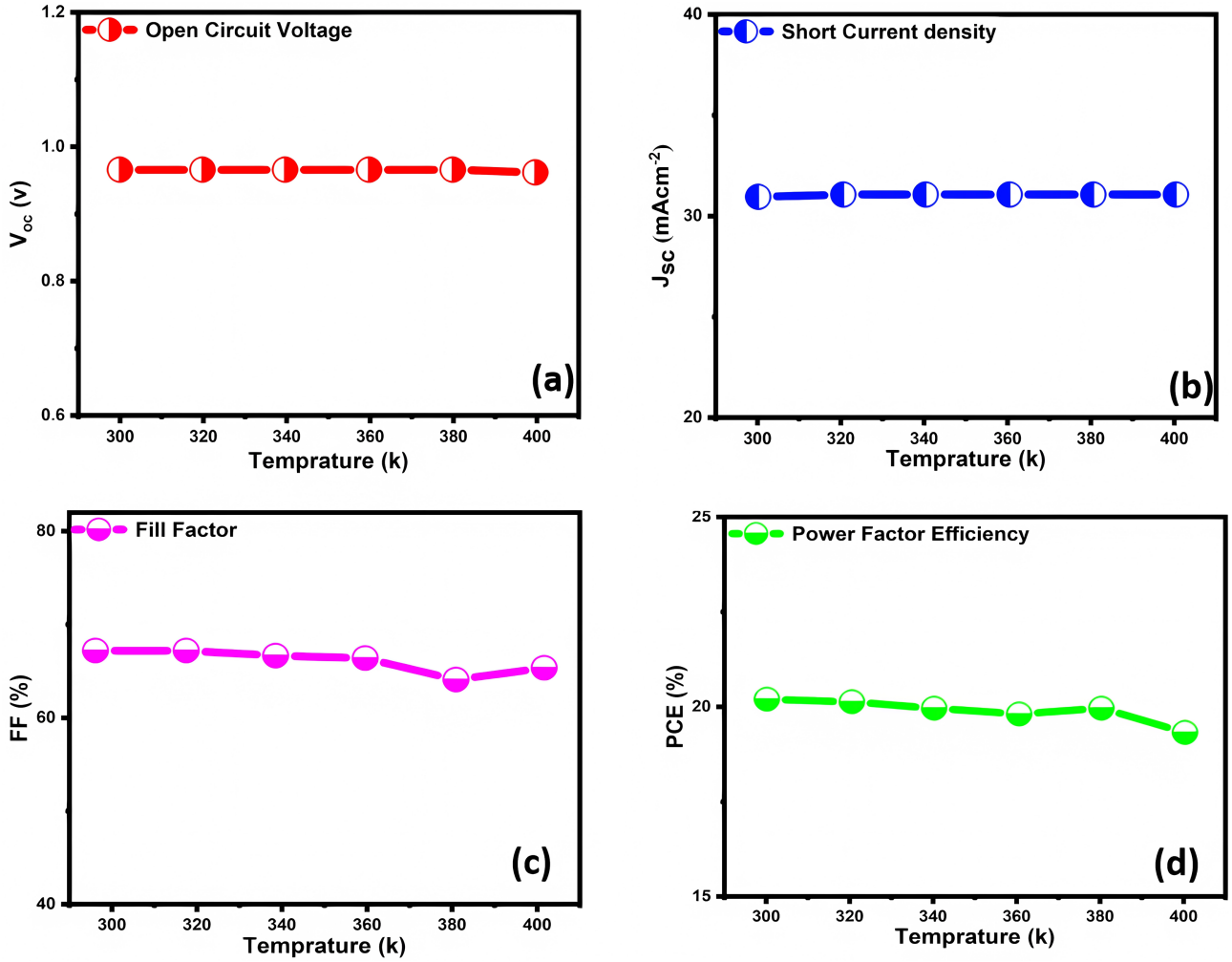

Figure 5. Influence of temperature on OSCs parameters (a) V_{oc}, (b) J_{sc}, (c) FF and (d) PCE.

Table 3. Output parameters of stimulated various temperature.

Temp (K)	V_{oc} (V)	J_{sc} (mAcm^{-2})	FF (%)	PCE (%)
300	0.964	31.049	67.61	20.25
320	0.964	31.051	67.54	20.23

Continued

340	0.963	31.049	67.12	20.09
360	0.962	31.048	66.58	19.90
380	0.961	31.043	65.00	19.96
400	0.958	31.037	65.43	19.47

3.3. Impact of Working Temperature on Series and Shunt Resistance: Insights from Impedance Spectroscopy

Impedance spectroscopy has been widely employed to explore the electrical characteristics of materials or devices. Electrochemical impedance spectroscopy (EIS) is a standard and popular method of the study of charge transport, recombination, and interfacial processes in semiconductor devices, such as organic solar cells [44]. In these devices, the frequency-dependent resistive and capacitive responses are caused by transport of charge carriers by semiconducting layers and charge concentration at interfaces [45]. The presence of distinct semicircles in Nyquist plots is widely attributed to different physical processes, with the high frequency semicircle linked to charge transport or series resistance, and the low frequency semicircle linked to recombination and interfacial dynamics of charge [46]. It follows that series resistance, charge transport or recombination resistance and capacitive (or constant phase) element models of equivalent circuit have been widely used to model the behavior of semiconductor junctions in organic photovoltaic devices. The circuit model used herein is thus in line with the accepted interpretations of impedance spectra in organic solar cells and has previous literature backing it [47]. This method helps study the impact of series resistance (R_s) and shunt resistance (R_{sh}) arising from interfaces and electrodes in a solar cell. Moreover, some of the capacitance in solar cells is undesirable, and this technique can be used to identify it. The process involves applying a low-level alternating current signal to the solar cell, with the signal frequency dependent on the area of investigation [48]-[50]. The impedance spectra of the OSCs are subsequently recorded at different working temperatures. (**Table 4**) Analyzing the impedance spectra within a specific frequency range provides essential information regarding the electrical properties of the OSCs. **Figure 6** shows a Nyquist plot's general representation, allowing us to determine R_s and R_{sh}.

The Nyquist plot of an ideal parallel R-C circuit shows a semicircle shape where each point corresponds to a specific frequency. At low frequencies, characterized by high values, it is possible to determine the combined resistance of the R_s within the intermediate frequency range, half of the R_s and R_{sh} components [51] [52]. Alternatively, can be determined by measuring the distance from the onset to the minimum point of the semicircle on the axis or by evaluating the absolute value of the reactance at the minimum of the semicircle. Additionally, the capacitive elements, such as the barrier capacitance (Cb), can be accessed at the angular frequency (ω) when it reaches its most negative value. **Figure 7** shows the Nyquist

plot of PM6:Y6-based OSCs at different working temperature. Two semicircles were observed. The small semicircle at the low value shows the contribution from the electrodes, while the large semicircles show the contribution from the semiconductor materials. Figure 8(a) and Figure 8(b) clearly show that the conductivity due to small semicircles decreases with the working temperature. In contrast, the conductivity of large semicircles increases with the working temperature, which indicates the metallic and semiconductor behavior, respectively [53] [54].

Table 4. Temperature dependents output values.

Temp (K)	R1	R2	CPE1-T	CPE2-T	CPE1-P	CPE2-P
300	1841	28.73	3.3449E−7	2.9651E−6	1.005	0.65535
320	1968	27.57	3.1416E−7	2.9294E−6	1.005	0.65835
340	2015	26.72	2.9943E−7	2.9918E−6	1.005	0.65775
360	2023	25.94	2.8808E−7	3.131E−6	1.006	0.65521
380	2007	25.27	2.7798E−7	3.3666E−6	1.006	0.65085
400	1975	24.66	2.6955E−7	3.6968E−6	1.006	0.64526

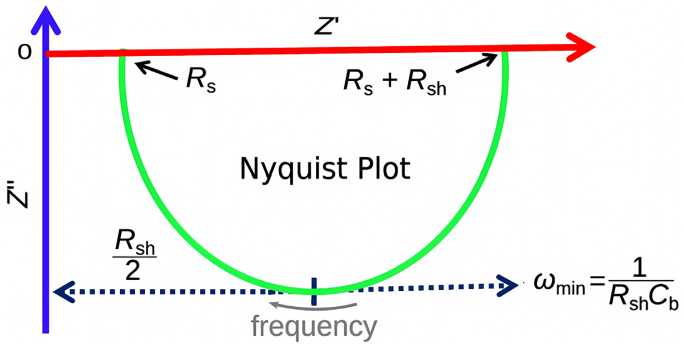

Figure 6. The general representation of a Nyquist plot.

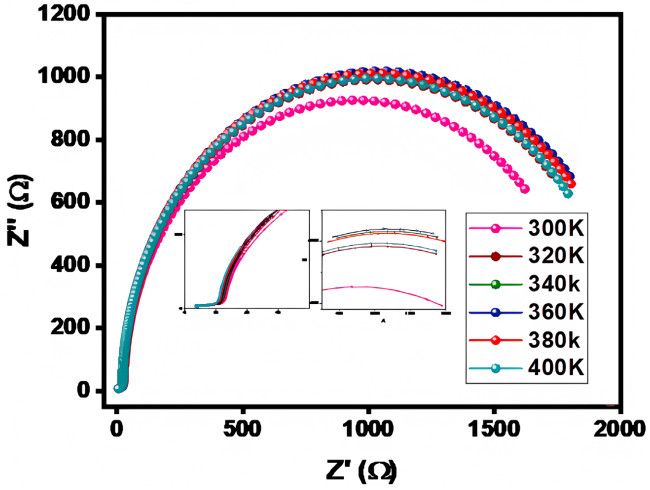

Figure 7. Nyquist graph of Impedance spectroscopy.

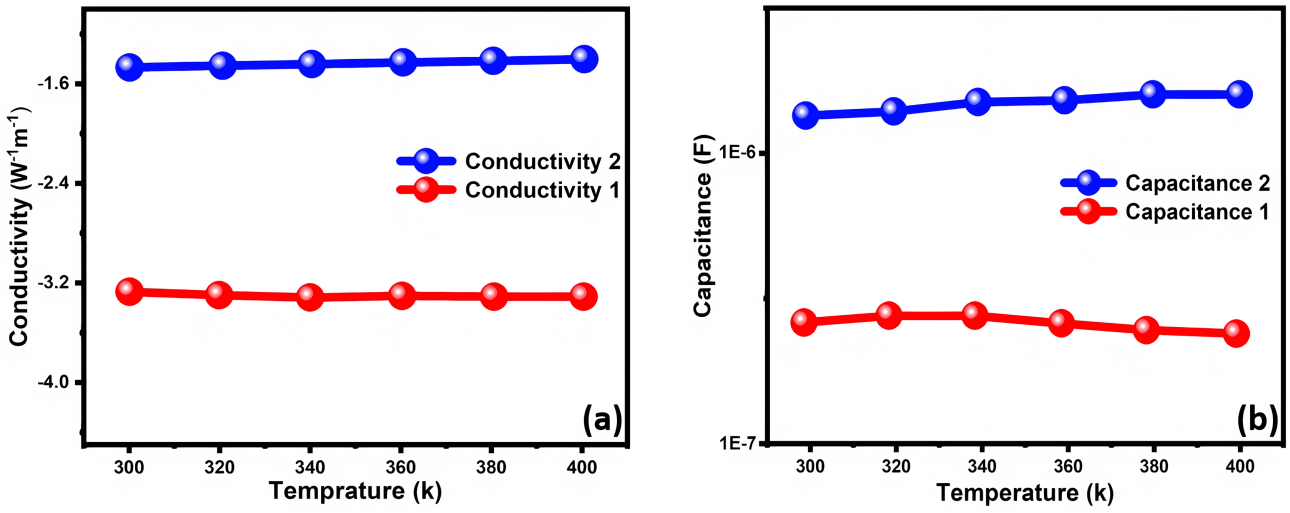

Figure 8. (a) The calculated conductivity and (b) Capacitance.

4. Conclusion

The study into the influence of active layer thickness and working temperature on the work of PM6:Y6-based organic solar cells is useful information that can help to optimize the performance of the device and learn how it will act in various operating conditions. When the active layer thickness is increased in 250 nm to 450 nm, the short-circuit current density (J_{sc}) is significantly improved because of the light absorption and exciton generation rate in the active layer. There is also a slight improvement in open-circuit voltage (V_{oc}) which can be attributed to the both preferred band structure and the alignment of the energy levels of the PM6:Y6 system. But at a critical active layer thickness of above 400 nm a critical drop of fill factor (FF) of 67.62 per cent to 65.8 per cent and power conversion efficiency (PCE) of 20.25 per cent to 20.08 per cent is recorded. This degradation is linked to a higher likelihood of charge carrier recombination that cancels the advantage of a high J_{sc} and a small increase in V_{oc}. In addition, the working temperature effects observation shows that J_{sc} proportional risen with temperature at first because of thermally activated conductivity and improved charge carrier generation and mobilities that plateaus at a specific temperature. Onward of its temperature, J_{sc} starts to fall since high temperatures adversely impact charge transportation and carrier lifetime. The V_{oc} steadily goes down as the temperature rises, mainly the narrowing of bandgaps and the rising carrier density. Unlike J_{sc}, FF and PCE are functions that decline with rising working temperature as the simulated results verify. This decrease is largely due to improved internal carrier recombination and heavier resistive losses in high temperatures which negatively impacts the charge extraction efficiency. Generally speaking, these results indicate that it is necessary to optimize the active layer thickness and operating temperature with care in order to obtain high-performance organic solar cells based on PM6:Y6. The findings are useful in designing and thermal engineering of inverted bulk heterojunction OSCs and in the development of efficient organic photovoltaic technologies.

Conflicts of Interest

The authors declare no conflicts of interest regarding the publication of this paper.

References

[1] Adak, S. (2025) Linearization of Photovoltaic Cell Single Diode Equivalent Circuit Model Using Piecewise Linear Parallel Branches Model and Findin Fill Factor. *Düzce Üniversitesi Bilim ve Teknoloji Dergisi*, **13**, 266-285. https://doi.org/10.29130/dubited.1502554

[2] Altındal, Ş., Karadeniz, S., Tuğluoğlu, N. and Tataroğlu, A. (2003) The Role of Interface States and Series Resistance on the I-V and C-V Characteristics in Al/SnO_2/p-Si Schottky Diodes. *Solid-State Electronics*, **47**, 1847-1854. https://doi.org/10.1016/s0038-1101(03)00182-5

[3] Nishat, S.S., Hossain, M.J., Mullick, F.E., Kabir, A., Chowdhury, S., Islam, S., *et al.* (2021) Performance Analysis of Perovskite Solar Cells Using DFT-Extracted Parameters of Metal-Doped TiO_2 Electron Transport Layer. *The Journal of Physical Chemistry C*, **125**, 13158-13166. https://doi.org/10.1021/acs.jpcc.1c02302

[4] Srivastava, K.V., Srivastava, P., Srivastava, A., Maurya, R.K., Singh, Y.P. and Srivastava, A. (2025) 1D TiO_2 Photoanodes: A Game-Changer for High-Efficiency Dye-Sensitized Solar Cells. *RSC Advances*, **15**, 4789-4819. https://doi.org/10.1039/d4ra06254j

[5] Hossain, M.K., Mohammed, M.K.A., Pandey, R., Arnab, A.A., Rubel, M.H.K., Hossain, K.M., *et al.* (2023) Numerical Analysis in DFT and SCAPS-1D on the Influence of Different Charge Transport Layers of $CsPbBr_3$ Perovskite Solar Cells. *Energy & Fuels*, **37**, 6078-6098. https://doi.org/10.1021/acs.energyfuels.3c00035

[6] Jiang, T., *et al.* (2025) Design and Optimization of Lead-Free Cs2$TiBr_6$/Cs_2SnI_6 Bilayer Perovskite Solar Cells for High Efficiency.

[7] Khan, S., Ullah, I., Khan, S., Ajmal, S., Saqib, N., Rahman, F.U., *et al.* (2024) Advancements in Nanohybrids: From Coordination Materials to Flexible Solar Cells. *Journal of Polymer Science and Engineering*, **7**, 4276. https://doi.org/10.24294/jpse.v7i1.4276

[8] Sahoo, P., Mishra, S.B., Debata, S., Sharma, A., Sahu, B.K., Padhan, S., *et al.* (2024) Hydrothermally Grown Halogen-Doped ZnO Nanorods for Photoelectrochemical Water Oxidation: Experimental and DFT Insights. *The Journal of Physical Chemistry C*, **128**, 18711-18723. https://doi.org/10.1021/acs.jpcc.4c03718

[9] Burgelman, M., Nollet, P. and Degrave, S. (2000) Modelling Polycrystalline Semiconductor Solar Cells. *Thin Solid Films*, **361**, 527-532. https://doi.org/10.1016/s0040-6090(99)00825-1

[10] Aliaghayee, M. (2023) Optimization of the Perovskite Solar Cell Design with Layer Thickness Engineering for Improving the Photovoltaic Response Using Scaps-1d. *Journal of Electronic Materials*, **52**, 2475-2491. https://doi.org/10.1007/s11664-022-10203-x

[11] Minemoto, T. and Murata, M. (2014) Device Modeling of Perovskite Solar Cells Based on Structural Similarity with Thin Film Inorganic Semiconductor Solar Cells. *Journal of Applied Physics*, **116**, Article ID: 054505. https://doi.org/10.1063/1.4891982

[12] Krebs, F.C. (2009) Fabrication and Processing of Polymer Solar Cells: A Review of Printing and Coating Techniques. *Solar Energy Materials and Solar Cells*, **93**, 394-412. https://doi.org/10.1016/j.solmat.2008.10.004

[13] Clarke, T.M. and Durrant, J.R. (2010) Charge Photogeneration in Organic Solar Cells. *Chemical Reviews*, **110**, 6736-6767. https://doi.org/10.1021/cr900271s

[14] Nelson, J. (2003) Diffusion-limited Recombination in Polymer-Fullerene Blends and Its Influence on Photocurrent Collection. *Physical Review B*, **67**, Article ID: 155209. https://doi.org/10.1103/physrevb.67.155209

[15] Yip, H. and Jen, A.K.-. (2012) Recent Advances in Solution-Processed Interfacial Materials for Efficient and Stable Polymer Solar Cells. *Energy & Environmental Science*, **5**, 5994-6011. https://doi.org/10.1039/c2ee02806a

[16] Kim, J.Y., Lee, K., Coates, N.E., Moses, D., Nguyen, T., Dante, M., *et al.* (2007) Efficient Tandem Polymer Solar Cells Fabricated by All-Solution Processing. *Science*, **317**, 222-225. https://doi.org/10.1126/science.1141711

[17] Dou, Q., Whatley, T., Syed, T., Wei, W. and Wang, H. (2022) Carbon Nanomaterials-Polymer Composites for Perovskite Solar Cells: Preparation, Properties and Applications. *Journal of Materials Chemistry A*, **10**, 19211-19230. https://doi.org/10.1039/d2ta02175g

[18] Sun, Y., Takacs, C.J., Cowan, S.R., Seo, J.H., Gong, X., Roy, A., *et al.* (2011) Efficient, Air-Stable Bulk Heterojunction Polymer Solar Cells Using MoO_x as the Anode Interfacial Layer. *Advanced Materials*, **23**, 2226-2230. https://doi.org/10.1002/adma.201100038

[19] Hau, S.K., Yip, H., Baek, N.S., Zou, J., O'Malley, K. and Jen, A.K. (2008) Air-Stable Inverted Flexible Polymer Solar Cells Using Zinc Oxide Nanoparticles as an Electron Selective Layer. *Applied Physics Letters*, **92**, Article ID: 253301. https://doi.org/10.1063/1.2945281

[20] Liu, Q., Jiang, Y., Jin, K., Qin, J., Xu, J., Li, W., *et al.* (2020) 18% Efficiency Organic Solar Cells. *Science Bulletin*, **65**, 272-275. https://doi.org/10.1016/j.scib.2020.01.001

[21] Zhang, M., Guo, X., Ma, W., Ade, H. and Hou, J. (2015) A Large-Bandgap Conjugated Polymer for Versatile Photovoltaic Applications with High Performance. *Advanced Materials*, **27**, 4655-4660. https://doi.org/10.1002/adma.201502110

[22] Guo, M., *et al.* (2025) Device Simulation of $BaZrSe_3$-Based Chalcogenide Perovskite Solar Cells with Back-Surface Field.

[23] Tress, W. (2014) Organic Solar Cells. In: Tress, W., Ed., *Organic Solar Cells*, Springer International Publishing, 67-214. https://doi.org/10.1007/978-3-319-10097-5_3

[24] Green, M.A. (1981) Solar Cell Fill Factors: General Graph and Empirical Expressions. *Solid-State Electronics*, **24**, 788-789. https://doi.org/10.1016/0038-1101(81)90062-9

[25] Luque, A. and Hegedus, S. (2011) Handbook of Photovoltaic Science and Engineering. John Wiley & Sons.

[26] Nelson, J. (2003). The Physics of Solar Cells. World Scientific Publishing Co. https://doi.org/10.1142/p276

[27] Green, M.A. (1982) Accuracy of Analytical Expressions for Solar Cell Fill Factors. *Solar Cells*, **7**, 337-340. https://doi.org/10.1016/0379-6787(82)90057-6

[28] Cheng, Y., Yang, S. and Hsu, C. (2009) Synthesis of Conjugated Polymers for Organic Solar Cell Applications. *Chemical Reviews*, **109**, 5868-5923. https://doi.org/10.1021/cr900182s

[29] Ali, N., Hussain, A., Ahmed, R., Wang, M.K., Zhao, C., Haq, B.U., *et al.* (2016) Advances in Nanostructured Thin Film Materials for Solar Cell Applications. *Renewable and Sustainable Energy Reviews*, **59**, 726-737. https://doi.org/10.1016/j.rser.2015.12.268

[30] Wibowo, A., Marsudi, M.A., Amal, M.I., Ananda, M.B., Stephanie, R., Ardy, H., *et al.* (2020) ZnO Nanostructured Materials for Emerging Solar Cell Applications. *RSC Advances*, **10**, 42838-42859. https://doi.org/10.1039/d0ra07689a

[31] Kim, S., Lee, J.K., Kang, S.O., Ko, J., Yum, J., Fantacci, S., *et al.* (2006) Molecular Engineering of Organic Sensitizers for Solar Cell Applications. *Journal of the American Chemical Society*, **128**, 16701-16707. https://doi.org/10.1021/ja066376f

[32] Beaujuge, P.M. and Fréchet, J.M.J. (2011) Molecular Design and Ordering Effects in Π-Functional Materials for Transistor and Solar Cell Applications. *Journal of the American Chemical Society*, **133**, 20009-20029. https://doi.org/10.1021/ja2073643

[33] Qi, B. and Wang, J. (2012) Open-Circuit Voltage in Organic Solar Cells. *Journal of Materials Chemistry*, **22**, 24315-24325. https://doi.org/10.1039/c2jm33719c

[34] Potscavage, W.J., Sharma, A. and Kippelen, B. (2009) Critical Interfaces in Organic Solar Cells and Their Influence on the Open-Circuit Voltage. *Accounts of Chemical Research*, **42**, 1758-1767. https://doi.org/10.1021/ar900139v

[35] Elumalai, N.K. and Uddin, A. (2016) Open Circuit Voltage of Organic Solar Cells: An In-Depth Review. *Energy & Environmental Science*, **9**, 391-410. https://doi.org/10.1039/c5ee02871j

[36] Widmer, J., Tietze, M., Leo, K. and Riede, M. (2013) Open-Circuit Voltage and Effective Gap of Organic Solar Cells. *Advanced Functional Materials*, **23**, 5814-5821. https://doi.org/10.1002/adfm.201301048

[37] Abbas, T. and Tahir, M. (2021) Tri-Metallic Ni-Co Modified Reducible TiO_2 Nanocomposite for Boosting H_2 Production through Steam Reforming of Phenol. *International Journal of Hydrogen Energy*, **46**, 8932-8949. https://doi.org/10.1016/j.ijhydene.2020.12.209

[38] Bowden, S. and Rohatgi, A. (2001) Rapid and Accurate Determination of Series Resistance and Fill Factor Losses in Industrial Silicon Solar Cells. Georgia Institute of Technology.

[39] Khanna, A., Mueller, T., Stangl, R.A., Hoex, B., Basu, P.K. and Aberle, A.G. (2013) A Fill Factor Loss Analysis Method for Silicon Wafer Solar Cells. *IEEE Journal of Photovoltaics*, **3**, 1170-1177. https://doi.org/10.1109/jphotov.2013.2270348

[40] Araujo, G.L., Cuevas, A. and Ruiz, J.M. (1986) The Effect of Distributed Series Resistance on the Dark and Illuminated Current—Voltage Characteristics of Solar Cells. *IEEE Transactions on Electron Devices*, **33**, 391-401. https://doi.org/10.1109/t-ed.1986.22500

[41] Green, M.A. (2016) Accurate Expressions for Solar Cell Fill Factors Including Series and Shunt Resistances. *Applied Physics Letters*, **108**, Article ID: 081111. https://doi.org/10.1063/1.4942660

[42] Tirado-Serrato, J.G., Garcia, A.S. and Maximov, S. (2024) Analytical Computation of the Maximum Power Point of Solar Cells Using Perturbation Theory. *Energies*, **17**, Article 6035. https://doi.org/10.3390/en17236035

[43] Hacke, P. and Meier, D. (2002) Analysis of Fill Factor Losses Using Current-Voltage Curves Obtained under Dark and Illuminated Conditions. *Conference Record of the Twenty-Ninth IEEE Photovoltaic Specialists Conference*, 2002, New Orleans, 19-24 May 2002, 462-464.

[44] Njema, G.G., Elmelouky, A., Meyer, E.L., Riouchi, N. and Kibet, J.K. (2025) Pioneering an Innovative Eco-friendly N719 Dye-sensitized Solar Cell through Modelling and Impedance Spectroscopy Analysis for Energy Sustainability. *Global Challenges*, **9**, e00276. https://doi.org/10.1002/gch2.202500276

[45] Guerrero, A., Loser, S., Garcia-Belmonte, G., Bruns, C.J., Smith, J., Miyauchi, H., *et al.* (2013) Solution-Processed Small Molecule: Fullerene Bulk-Heterojunction Solar Cells: Impedance Spectroscopy Deduced Bulk and Interfacial Limits to Fill-Factors. *Physical Chemistry Chemical Physics*, **15**, 16456. https://doi.org/10.1039/c3cp52363b

[46] Bisquert, J. (2001) Theory of the Impedance of Electron Diffusion and Recombination in a Thin Layer. *The Journal of Physical Chemistry B*, **106**, 325-333. https://doi.org/10.1021/jp011941g

[47] Fabregat-Santiago, F., Garcia-Belmonte, G., Mora-Seró, I. and Bisquert, J. (2011) Characterization of Nanostructured Hybrid and Organic Solar Cells by Impedance Spectroscopy. *Physical Chemistry Chemical Physics*, **13**, 9083-9118. https://doi.org/10.1039/c0cp02249g

[48] Macdonald, J.R., Johnson, W.B., Raistrick, I.D., Franceschetti, D.R., Wagner, N., McKubre, M.C.H., *et al.* (2018) Impedance Spectroscopy: Theory, Experiment, and Applications. John Wiley & Sons, 424-458. https://elib.dlr.de/121440/

[49] Kiermasch, D., Gil-Escrig, L., Bolink, H.J. and Tvingstedt, K. (2019) Effects of Masking on Open-Circuit Voltage and Fill Factor in Solar Cells. *Joule*, **3**, 16-26. https://doi.org/10.1016/j.joule.2018.10.016

[50] Kim, M., Kim, B. and Kim, J. (2009) Effective Variables to Control the Fill Factor of Organic Photovoltaic Cells. *ACS Applied Materials & Interfaces*, **1**, 1264-1269. https://doi.org/10.1021/am900155y

[51] Pysch, D., Mette, A. and Glunz, S.W. (2007) A Review and Comparison of Different Methods to Determine the Series Resistance of Solar Cells. *Solar Energy Materials and Solar Cells*, **91**, 1698-1706. https://doi.org/10.1016/j.solmat.2007.05.026

[52] Rahman, M.U., Usman, M., Sayyad, M.H. and Abbas, S.Z. (2024) Impact of Carbon Electrode Layer on the Series Resistance and Fill Factor of $Ch_3Nh_3PbI_3$ Perovskite Solar Cell. *Physica Scripta*, **99**, Article ID: 105974. https://doi.org/10.1088/1402-4896/ad75cd

[53] Greulich, J., Glatthaar, M. and Rein, S. (2012) Separation of Series Resistance and Space Charge Region Recombination in Crystalline Silicon Solar Cells from Dark and Illuminated Current-Voltage Characteristics. *IEEE Journal of Photovoltaics*, **2**, 241-246. https://doi.org/10.1109/jphotov.2012.2189370

[54] Yun, J., Lee, S., Jeong, M. and Lee, S.B. (2018) Influence of Die-Cast Rotor Fill Factor on the Starting Performance of Induction Machines. *IEEE Transactions on Magnetics*, **54**, 1-4. https://doi.org/10.1109/tmag.2017.2750101